Available online at www.sciencedirect.com

ScienceDirect

Journal of the European Ceramic Society 34 (2014) 4037–4042

www.elsevier.com/locate/jeurceramsoc

Compressive creep testing of refractories at elevated loads—Device, material law and evaluation techniques

Shengli Jin *, Harald Harmuth, Dietmar Gruber

Montanuniversität Leoben, A-8700 Leoben, Austria

Received 19 March 2014; received in revised form 21 May 2014; accepted 23 May 2014
Available online 17 June 2014

Abstract

In order to cost-effectively characterize the high temperature compressive creep behaviour of refractories a testing device was designed for application at elevated loads. Special measures have been taken necessary to enable an even stress distribution within the specimen. To identify Norton-Bailey strain hardening creep law parameters a general inverse procedure using a Levenberg–Marquardt algorithm was developed. Satisfying experimental results could be received from the creep measurement in a wide range of temperatures and loads for both shaped and unshaped materials. By fitting the strain/time curves the creep law parameters of refractories under various temperatures can be precisely identified. The measurements also reveal that at elevated loads all three creep stages can be observed.

Keywords: Compressive creep; Elevated loads; Norton-Bailey; Inverse estimation; Refractories

1. Introduction

During service refractories are frequently exposed to intense thermomechanical loads resulting from the collaborative effects of severe thermal shock, thermal expansion of refractories and external mechanical constraints.[1,2] Under these conditions refractories may respond in elastic or inelastic manner which depends on the magnitudes and types of loads as well as on the material behaviour at high temperatures. Both material failure under Mode I–III conditions and creep may account for this inelastic behaviour and bring about an irreversible deformation of refractories.[3–7]

To characterize the creep behaviour of refractories, conventionally two types of testing procedures are employed. One is so called creep-in-compression (abbreviated as CIC) which applies the same equipment as the testing procedure for refractoriness-under-load (abbreviated as RUL). The standards of CIC in Europe, USA, Japan and China are more or less similar and mainly differ in specimen dimension, testing load and heating rate.[8] According to the European standard EN 993-9,[9] a fixed compressive stress of 0.2 MPa is loaded on the specimen during the heating-up and dwell periods. The change in length of the specimen is measured from the differential displacement of two corundum tubes through linear variable differential transducers (LVDTs). The deformation at certain dwell time relative to the maximum expansion occurring during the heating-up period is determined. This method is applied to compare the creep resistance capacity of refractories and to receive guidance for material selection and development in a rather phenomenological manner.[10–13] However, a deeper understanding of the creep mechanisms of refractories is demanded as well as extracting creep data for further thermomechanical modelling. For this purpose various loading conditions were also considered.[14–19] Formulating the secondary creep rate in dependence of temperature and stress offers one way to reveal the creep mechanisms of refractories, from which measures for material improvement may follow.

What are the tasks a satisfactory creep testing equipment should fulfil? The CIC measurement according to the European standard EN 993-9 is not suitable for determination of creep

* Corresponding author. Tel.: +43 038424023236; fax: +43 038424023201.
E-mail address: shengli.jin@unileoben.ac.at (S. Jin).

http://dx.doi.org/10.1016/j.jeurceramsoc.2014.05.034
0955-2219/

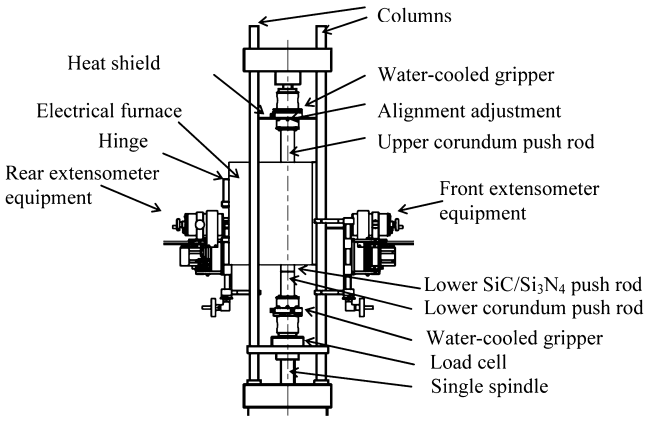

Fig. 1. Schematic diagram of the testing machine.

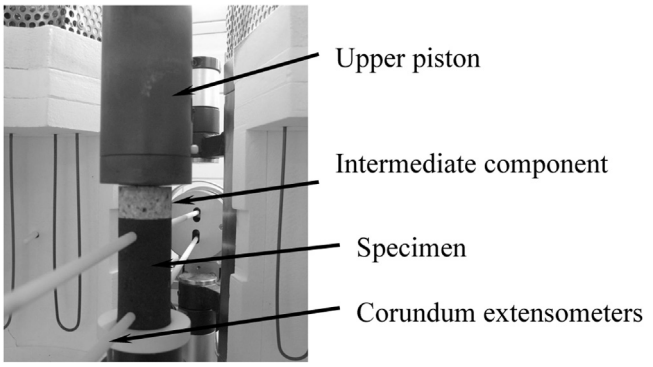

Fig. 2. Setup of the high temperature compressive creep test in the furnace.

laws. One reason is that the onset of creep is not defined. Creep will start during the heating up procedure before the beginning of the dwell time because the specimen is heated up under load. Moreover the restriction of the maximum load to 0.2 MPa does not allow investigation of load levels significant for practical use of refractories in many cases. A newly designed testing equipment should especially allow the following features of the measurement: The start of the loading under isothermal conditions must be defined exactly. Moreover, displacement has to be measured on the specimen surface itself, preferably at least at two diametrical locations, in order to assess even creep of the material. Further alignment of the specimen and the testing machine is of high importance: the line of action of the imposed load has to coincide with the specimen axis. Otherwise a bending moment would be caused and result in an uneven stress distribution within the specimen. Moreover a homogenous load distribution will depend on the quality of the specimen preparation; especially parallel end faces perpendicular to the specimen axis are desired. Furthermore the application of sufficiently high stresses related to service conditions is necessary. Only sufficiently high load levels will allow observing secondary and tertiary creep in reasonable testing times.

To fulfil these missions a testing device for high temperature compressive creep application was newly developed and is presented in this paper. Efficient inverse procedure to identify the creep law parameters is also introduced with two case studies of shaped and unshaped materials.

2. Construction and main features of the testing machine

A schematic diagram of the device for high temperature compressive creep testing is shown in Fig. 1. The whole setup is based on a spindle-driven universal testing machine of sufficient stiffness. An electrical furnace is inserted and equipped with silicon carbide heating elements. The furnace is composed of two symmetrical parts, held together by means of hinges in the rear and can be closed tightly with two buckles in the front. Two platinum-rhodium thermocouples are used to measure the temperatures, one of which is located near the specimen to monitor its temperature and the other one is placed close to the heating elements to control the furnace temperature. Two pairs of corundum extensometers are placed in the front and rear of the furnace, respectively. The loading is realized by a single spindle connected to a load cell. Water-cooled grippers are placed at the cold ends of corundum push rods to protect the metal components. To guarantee coincidence of the axis of the lower and upper piston an alignment adjustment is provided.

Compared to conventional creep testing machines, this device possesses several advanced characters: compared with the CIC test it allows application of by far higher loads up to app. 20 MPa on a specimen with a diameter of 35 mm and a height of 70 mm. The height/diameter ratio of 2 is suitable for deformation measurement in a zone of the specimen which is not affected from friction of the end faces (here especially the lower end face) any more. The displacement of the specimen under load is measured directly on its surface utilizing two pairs of corundum extensometers, as seen in Fig. 2; the onset of deformation measurement is documented while the loading procedure starts, and therefore the point of creep origin is well defined. Uneven loading is tactically avoided by modifying the end face of the upper piston into a slight spherical surface. Both end faces of the cylindrical specimens are prepared by diamond grinding. Point-surface contact between the upper rod and the specimen would result in a concentrated load on both surfaces. In order to protect the head of upper ceramic rod and load the force evenly onto the specimen, a less brittle refractory material is placed between the ceramic rod and specimen, as labelled as intermediate component in Fig. 2.

Alignment of specimen and testing machine is essential to achieve similar readings on both extensometers. Therefore the specimen axis has to coincide with the line of action of the applied load. This can be tested by preloading at room temperature before starting the test. Necessary alignment can be done by adjusting the position of the upper piston (alignment adjustment in Fig. 1) or of the specimen itself. The creep tests will normally be performed under isothermal conditions after the furnace is heated up to a defined temperature with 10 K/min. In order to fix the specimen a small preload is applied before the temperature is achieved. Afterwards, the loading procedure is commenced by ascending the lower crosshead; a heading of 0.3 mm/min is mainly applied. The creep test under constant load will last several hours. The extensometer reading starts from the beginning of loading with an initial leg distance of up to 50 mm between

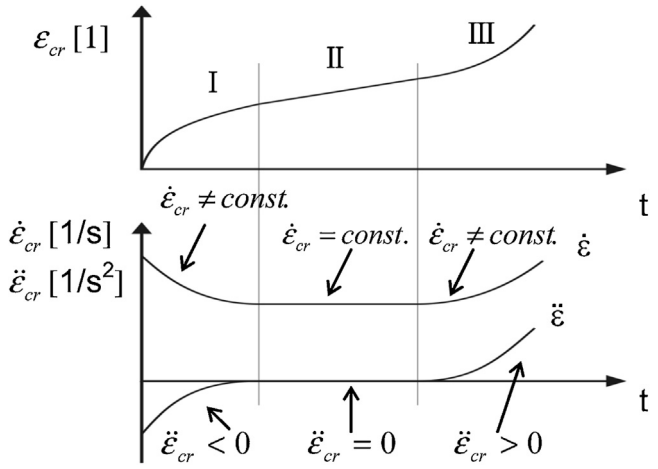

Fig. 3. Creep strain (ε_{cr}), strain rate ($\dot{\varepsilon}_{cr}$) and acceleration of creep strain ($\ddot{\varepsilon}_{cr}$) curves including three stages. (I) primary creep, (II) secondary creep, (III) tertiary creep.

two extensometer tips at each side. The measurement results of extensometers include the elastic and creep deformation during the loading procedure and the period with constant load.

3. Norton-Bailey creep law and inverse estimation procedure

Generally a complete creep strain/time curve under a constant load and temperature can be divided into three stages. As illustrated in Fig. 3, the first stage is called primary creep and characterized by time-dependent creep strain rate ($\dot{\varepsilon}_{cr}$) which decreases with time ($\ddot{\varepsilon}_{cr} < 0$). Following it the secondary creep shows a constant creep strain rate which is the minimum one of all three stages. Tertiary creep is characterized by a rising strain rate ($\ddot{\varepsilon}_{cr} > 0$) and leads to failure.

Many suggestions were given to describe the material creep behaviour in terms of stress, time and temperature based on uniaxial tests, among which the Norton-Bailey creep law is widely applied.[20] This law may be expressed as time-hardening/softening and strain hardening/softening formulations. At a constant stress history both formulations predict the same results. However, for a variable stress history the strain hardening formulation was proved to give a better agreement with the experimental creep curves.[20] According to the Norton-Bailey strain hardening/softening formulation, the creep strain rate is a function of temperature, stress and creep strain:

$$\dot{\varepsilon}_{cr} = K(T) \cdot \sigma^n \cdot \varepsilon_{cr}^a \tag{1}$$

here K is a temperature function, n the stress and a the creep strain exponent. The value of a is negative in the case of strain hardening (primary creep) and positive for strain softening (tertiary creep). For $a = 0$ secondary creep is represented.

As mentioned before, the measured results contain both elastic and creep deformation. To obtain the creep strain ε_{cr}, the total strain ε_{tot} is firstly calculated from the experimental deformation taking into account the initial extensometer legs distance (50 mm), and then the elastic strain σ/E is subtracted.

$$\varepsilon_{cr} = \varepsilon_{tot} - \frac{\sigma}{E} \tag{2}$$

here σ is the applied stress and E the Young's modulus which can be determined by IET (Impulse excitation technique) measurement.[21]

In order to inversely identify the parameters of Norton-Bailey creep law Eq. (1) was rearranged separating the variables ε_{cr} and t and then integrated. In the special case of predefined stress/time curves followed by the testing machine control unit the integration of σ^n with respect to time can easily be done analytically. This especially holds for a linear stress increase followed by a constant value as it was applied for the measurements documented here. For non predefined stress/time curves, e.g. if the strain is preset, a numerical integration is performed. Applying the trapezoidal rule for sufficiently low intervals between successive time steps t_{i+1} and t_i then gives:

$$\varepsilon_{cr,i+1} \approx \left[\varepsilon_{cr,i}^{1-a} + \frac{(1-a) \cdot K \cdot (\sigma_{i+1}^n + \sigma_i^n) \cdot (t_{i+1} - t_i)}{2} \right]^{1/1-a} \tag{3}$$

here the subscripts $i+1$, i of strain and stress refer to the respective time steps. For inverse identification of creep parameters the sum of the squared differences of measured and simulated strain has been minimized. Two algorithms have been used for this purpose, a Generalized Reduced Gradient method[22] and a Levenberg–Marquardt optimization technique.[23] The latter one was finally chosen due to its favourable convergence and was realized by combining Matlab (Version 7.11.0, MathWorks) with a Python file for the discretization of experimental data.

4. Results

4.1. Creep of burnt refractory bricks

Cylinder specimens as defined above have been prepared from commercially available burnt magnesia-chromite bricks (56.6 wt% MgO, 25.5 wt% Cr_2O_3). During the heating-up period, 100 N (equivalent to 0.1 MPa) was loaded axially on the specimen in order to fix it. Once the target temperature was reached, the extensometers were attached to the specimen before the loading procedure started. A total strain/time curve under constant load was obtained after 5 h. The measurements were carried out at 1100–1550 °C under various loads. Fig. 4 shows the curves measured at 1100–1300 °C with loads of 5 MPa, 7 MPa and 9 MPa necessary to provoke an evident creep of burnt magnesia-chromite specimen. As seen in Fig. 4, the ultimate total strains at 1100 °C and 1200 °C under a stress of 5 MPa are still quite small. Increased deformation can be observed when the load was elevated to yield 7 or 9 MPa. At 1300 °C with only 5 MPa a higher creep was observed than that at lower temperatures with up to 9 MPa. Further increasing the testing temperature to 1400 °C at the same load resulted in a dramatic increase of the ultimate total strain to a value more than 5 times of that at 1300 °C under the same load (Fig. 5). When the

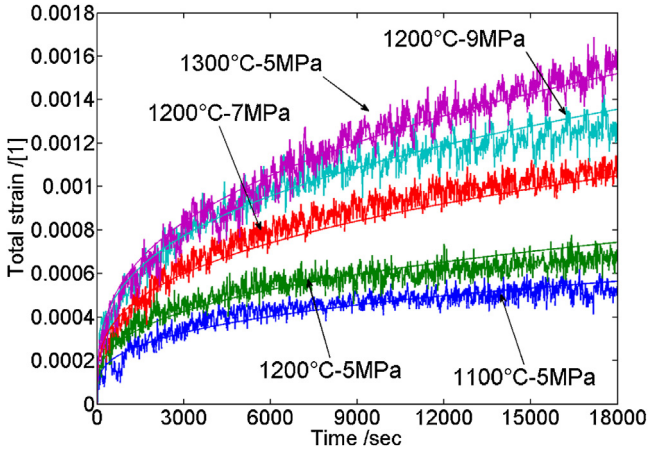

Fig. 4. Total strain/time curves of burnt magnesia-chromite bricks from experiments (fluctuating ones) and inverse estimations (smooth ones) at 1100–1300 °C.

temperature is higher than 1400 °C, even by applying loads less than 3 MPa a high deformation still can be received.

The curves obtained for 1100–1300 °C were used to compare the capacity of the two optimization algorithms quoted above, and the identified results are listed in Table 1. The creep of magnesia-chromite bricks shares the same values of n and a at these three temperatures. As expected both methods show consistent results of n and a with deviation of 1.7% and 2.8%, respectively. Temperature-dependent coefficient K shows larger deviations. The approach applying the Generalized Reduced Gradient algorithm used an analytical integration of σ^n as quoted above valid for the specific loading procedure with a linear increase of stress up to a constant level. The Generalized Reduced Gradient minimization exhibits to be more sensitive with respect to initial values compared with the Levenberg–Marquardt method. The convergence of the latter less depends on the initial values. As seen in Fig. 6, poor initial creep law parameters were given (K is 0.1 $MPa^{-n}\,s^{-1}$, n is 20 and a is −20). A steep decrease of the residual is observed for the first 12 iterations and after 20 iterations the optimised creep law parameters are found with sufficient accuracy.

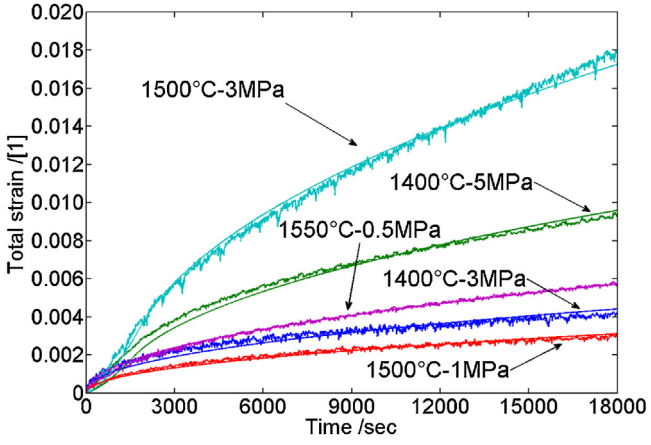

Fig. 5. Total strain/time curves of burnt magnesia-chromite bricks from experiments (fluctuating ones) and inverse estimations (smooth ones) at 1400–1550 °C.

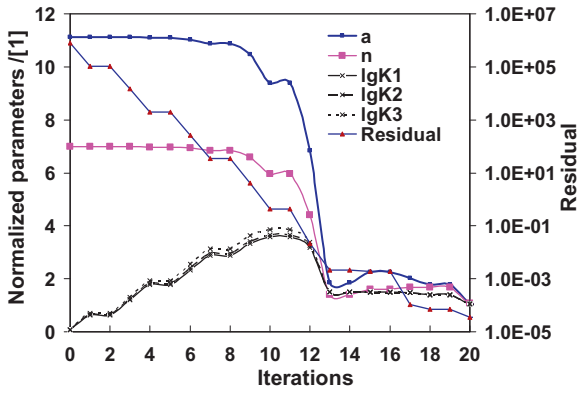

Fig. 6. The convergence behaviour of Levenberg–Marquardt method for inverse identification of the creep parameters.

Further identification by Levenberg–Marquardt method for the measurements at 1400–1550 °C was carried out and the corresponding identified parameters are given in Table 1 as well. The calculated total strains for the temperatures 1100–1550 °C were plotted versus testing time in Figs. 4 and 5 and show a satisfying agreement with the measurement. It can be concluded that creep behaviour of the magnesia-chromite bricks investigated here largely changes around 1400 °C. As seen in Table 1, the value of K for 1400 °C is four powers of ten larger than that for 1300 °C, while the value of n for 1400–1550 °C is only slightly higher than that for 1100–1300 °C and the value of a for 1400–1550 °C is only 58% of that for 1100–1300 °C. It is worth mentioning that for all of the measurements shown in Figs. 4 and 5 the creep of the investigated materials is still at the primary stage since the values of a are negative at all the testing temperatures.

At 1400 °C for a load of 9 MPa a typical total strain/time curve including all three creep stages was obtained, as seen in Fig. 7. A fit based on Norton-Bailey creep law has been applied to identify these three stages. For the primary creep stage the creep parameters shown in Table 1 have been obtained. In the case of secondary creep, the exponent of creep strain a is zero and only the value of $K_2\sigma^{n2}$ could be inversely calculated from this curve. At the third stage, both a_3 and $K_3\sigma^{n3}$ were inversely

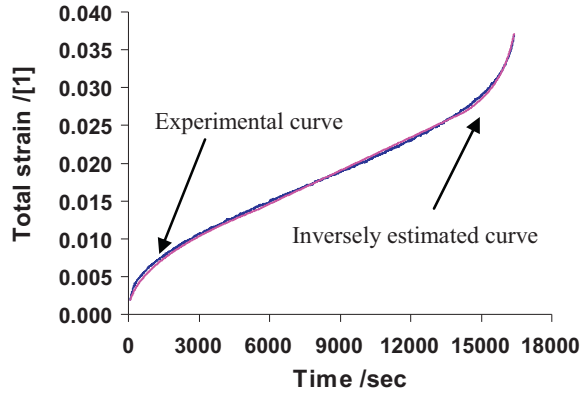

Fig. 7. A total strain/time curve of burnt magnesia-chromite bricks from the experiment and inverse estimation including three creep stages at 1400 °C under 9 MPa.

Table 1
Norton-Bailey creep law parameters of burnt magnesia-chromite bricks corresponding to different temperatures.

T (°C)	L–M	GRG	L–M	GRG	L–M	GRG
	K (MPa^{-n} s^{-1})		n		a	
1100	1.18×10^{-16}	0.71×10^{-16}				
1200	2.77×10^{-16}	1.72×10^{-16}	2.86	2.91	−1.80	−1.85
1300	2.33×10^{-15}	1.47×10^{-15}				
1400	1.24×10^{-11}	–				
1500	2.20×10^{-10}	–	3.20	–	−1.04	–
1550	7.27×10^{-9}	–				

L–M: Levenberg–Marquardt method.
GRG: Generalized Reduced Gradient method.

Table 2
Norton-Bailey creep law parameters of three stages of burnt magnesia-chromite bricks.

Creep law parameter	a_1	$K_1\sigma^{n1}$ (s^{-1})	a_2	$K_2\sigma^{n2}$ (s^{-1})	a_3	$K_3\sigma^{n3}$ (s^{-1})
Value	−1.04	1.44×10^{-8}	0	1.47×10^{-6}	6.3	1.58×10^{4}

estimated. The corresponding creep law parameters are listed in Table 2. It can be seen that the value of $K_2\sigma^{n2}$ is two orders of magnitude larger than $K_1\sigma^{n1}$. Assuming the same stress exponent for the primary and secondary creep K_2 should be equal to $K_1\varepsilon_{cr}^{a}$ where ε_{cr} is given as the ultimate creep strain of the primary stage. Actually they differ by only approximately 15% which is acceptable considering the deviation of displacement measurements.

The following considerations concern the possible determination of creep mechanisms from the creep rate law. Normally secondary creep is applied for this purpose.[24] Secondary creep strain rate is then assumed to be proportional to powers of the grain size and the stress. Creep mechanisms are revealed from the stress exponent, the grain size exponent and the activation energy for the diffusion process which are determined from the proportionality constant. If a grain size exponent is not known, still lattice mechanisms could be revealed. As secondary creep often is not observed[25,26] the question arises whether Norton-Bailey law for primary creep might be applied for this purpose. Particularly the apparent activation energy could only be calculated from K_1 under the following restrictions: the stress exponent is the same in primary and secondary stage and the ultimate creep strain of primary stage is constant, viz. it does not change with temperature or load. These conditions have not been verified so far, and therefore material laws established here have not been applied for investigation of creep mechanisms. It would give a deep insight to understand the creep behaviour of refractories by distinguishing the transition points of three creep stages, as well as the corresponding creep law parameters.

4.2. Creep of unshaped refractories

An ultra-low cement high alumina castable was selected for the creep study. It contains 92 wt% Al_2O_3, 6.0 wt% SiO_2 and 1.5 wt% CaO. The virgin castable after curing at 110 °C was heated up to the defined temperature with a preload as small as 5 N (equivalent to 5 kPa), and then held for 3 h in order to achieve thermal and phase equilibria. The experimental total strain/time curves for 1200–1500 °C were plotted in Fig. 8. It can be seen that the high alumina castable shows higher ultimate deformation after 5 h measurement under 0.2 MPa at 1300 °C in comparison to that under 1.5 MPa at 1400 °C. XRD analysis shows that the specimens tested at 1300 °C consist of corundum, anorthite, quartz and cristobalite, whilst the specimens tested at 1400 °C comprise only corundum and mullite. It is assumed that the higher creep at 1300 °C is related to the fact that the material is still not in equilibrium. It contains silica carriers added at room temperature and not in equilibrium with alumina. Equilibration might bring about enhanced diffusion processes, sintering and shrinkage and possibly the formation of intermediate liquid phases. This gives rise to higher creep. At 1400 °C equilibration is already finished and mullite already crystallized contributes to lower creep of castable. In this case if 0.2 MPa was previously added on the specimen during heating up to 1400 °C, definitely significant creep strains will be developed around 1300 °C. This will affect the determination of creep laws out of the experimental curves.

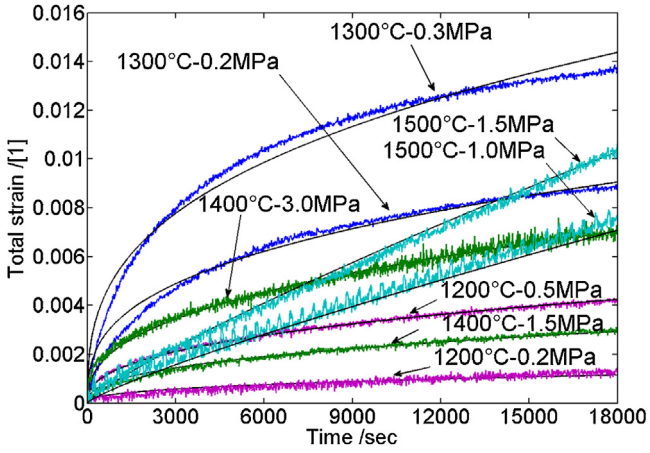

Fig. 8. Total strain/time curves of alumina castable from experiments (fluctuating ones) and inverse estimations (smooth ones) at 1200–1500 °C.

Table 3
Norton-Bailey creep law parameters of alumina castable at 1200–1500 °C.

T (°C)	K (MPa^{-n} s^{-1})	n	a
1200	2.41×10^{-10}	3.59	−1.57
1300	7.24×10^{-9}	3.51	−1.93
1400	5.69×10^{-12}	2.38	−1.53
1500	1.35×10^{-7}	1.14	−0.18

The creep law parameters of K, n and a were inversely estimated by Levenberg–Marquardt method and listed in Table 3. Values of n and a at 1200 °C and 1300 °C are quite close, but the value of K at 1300 °C is one order of magnitude higher than that at 1200 °C. Since the castable has higher creep resistance at 1400 °C, a decrease of K and n can be found. At 1500 °C, the castable shows highest value of K, with n close to 1 and a approaching zero. It illustrates that not only K but also n and a are temperature dependent, mainly because the virgin castable experiences sintering, chemical reaction or phase evolution at various temperatures. Similarly as for the burned magnesia-chromite bricks, the a values of high alumina castable are still negative and indicates that only primary creep stage was revealed in Fig. 8.

5. Conclusions

The new high temperature compressive creep testing device can be used to characterize the creep behaviour of shaped and unshaped materials at elevated loads. A preload of 0.2 MPa as applied for CIC measurements cannot be used during the heating up procedure for unshaped materials since these materials show inferior creep resistance especially at intermediate temperatures if they have not been fired before. Creep law parameters inversely identified by Levenberg–Marquardt method imply that both materials did not reach secondary creep under the specified loads in 5 h. However, by further elevating the load three stages of creep were obtained and distinguished as Norton-Bailey type creep. Additional to the elevated temperature and loads, also increasing the loading time in a reasonable scale may give rise to three stages of creep. Determination of transition points of three stages is necessary to understand the impacts of temperature, stress and creep strain on the creep behaviour of refractories. This is an item for the further research.

Acknowledgements

Financial support by the Austrian Federal Government and the Styrian Provincial Government (Grant no. A4.15) (Österreichische Forschungsförderungsgesellschaft and Steirische Wirtschaftsförderungs-gesellschaft) within the K2 Competence Centre on Integrated Research in Materials, Processing and Product Engineering (MCL Leoben) in the framework of the Austrian COMET Competence Centre Programme is gratefully acknowledged.

Appendix A. Supplementary data

Supplementary material related to this article can be found, in the online version, at http://dx.doi.org/10.1016/j.jeurceramsoc.2014.05.034.

References

1. Jin S, Harmuth H, Gruber D. Classification of thermomechanical impact factors and prediction model for ladle preheating. *J Wuhan Univ Sci Technol* 2011;**34**(1):28–31.
2. Jin S, Auer T, Gruber D, Harmuth H, Frechette MH, Li Y. *Thermo-mechanical modelling of steel ladle process cycles. Interceram, Refractories Manual*, vol. 1; 2012. p. 37–41.
3. Jin S, Gruber D, Harmuth H, Frechette MH. Thermomechanical steel ladle simulation including a Mohr–Coulomb plasticity failure model. *RHI Bull* 2012;**2**:39–43.
4. Gruber D, Harmuth H, Andreev K. FEM simulation of the thermomechanical behaviour of the refractory lining of a blast furnace. *J Mater Process Technol* 2004;**155–156**:1539–43.
5. Andreev K, Harmuth H. FEM simulation of the thermo-mechanical behaviour and failure of refractories-a case study. *J Mater Process Technol* 2003;**143–144**:72–7.
6. Chen E, Buyukozturk O. Methodology for thermomechanical analysis of brittle system. *Am Ceram Soc Bull* 1985;**64**(7):982–8.
7. Chen E, Buyukozturk O. Thermomechanical behavior and design of refractory linings for slagging gasifiers. *Ceram Bull* 1985;**64**(7):988–94.
8. Matsumura I, Hayashi Y, Hiyama Y, Ijiri A. Refractoriness under load and hot creep measurements. *Taikabutsu Overseas* 1990;**2**(2):36–42.
9. EN 993-9. *Methods of test for dense shaped refractory products. Determination of creep in compression*; 1973.
10. Diaz LA, Torrecillas R. Hot bending strength and creep behaviour at 1000–1400 °C of high alumina refractory castables with spinel, periclase and dolomite additions. *J Eur Ceram Soc* 2009;**29**(1):53–8.
11. Terzic A, Pavlovic L, Milutinovic-Nikolic A. Influence of the phase composition of refractory materials on creep. *Sci Sinter* 2006;**38**(3):255–63.
12. Jokanovic V, Djurkovic G, Curcic R. Creep and microstructure in refractory materials. *Am Ceram Soc Bull* 1998;**77**(7):61–5.
13. Chien Y, Lee T, Pan H, Ko Y. Effect of Cr_2O_3 on creep resistance of high alumina bauxite refractories. *Ceram Bull* 1984;**63**(7):915–8.
14. Hemrick JG, Wereszczak AA. Non-classical creep behaviour of fusion-cast α-β alumina refractories. *Refract Appl Trans* 2009;**4**(1):2–8.
15. Krause RF. Compressive strength and creep behaviour of a magnesium chromite refractory. *Ceram Eng Sci Proc* 1986;**7**(1,2):220–8.
16. Wereszczak AA, Kirkland TP, Curtis WF. Creep of CaO/SiO_2-containing MgO refractories. *J Mater Sci* 1999;**34**:215–27.
17. Bray DJ, Smyth JR, McGee TD, Kim G. Effect of cement content on the creep of a 90+% Al_2O_3 refractory concrete. *Ceram Bull* 1984;**63**(2):287–9.
18. Bray DJ, Smyth JR, McGee TD. Thermal/strain history effects on creep of refractory concrete. *J Am Ceram Soc* 1982;**65**(6):275–9.
19. Bray DJ, Smyth JR, McGee TD. Creep of 90+%Al_2O_3 refractory concrete. *Ceram Bull* 1980;**59**(7):706–10.
20. Boyle JT, Spence J. *Stress analysis for creep*. England: Butterworths; 1983.
21. Roebben G, Bollen B, Brebels A, Van Humbeeck J, Van der Biest O. Impulse excitation apparatus to measure resonant frequencies: elastic moduli, and internal friction at room and high temperature. *Rev Sci Instrum* 1997;**68**(12):4511–5.
22. Lasdon LS, Waren AD, Jain A, Ratner M. Design and testing of a generalized reduced gradient code for nonlinear programming. *ACM Trans Math Soft* 1978;**4**(1):34–50.
23. Marquardt DW. An algorithm for least-squares estimation of nonlinear parameters. *J Soc Ind Appl Math* 1963;**11**(2):431–41.
24. Canon WR, Langdon TG. Creep of ceramics. Part 1. Mechanical characteristics. *J Mater Sci* 1983;**18**:1–50.
25. Dixon-Stubbs PJ, Wilshire B. High temperature creep behaviour of a fired magnesia refractory. *Trans J Br Ceram Soc* 1981;**80**:180–5.
26. Evans RW, Scharning PJ, Wilshire B. Creep of CaO/MgO refractories. *J Mater Sci* 1985;**20**:4163–8.